MCAT Institute
Progress Report
93-10

Supersonic Airplane Study and Design

Samson Cheung

June 1993

NCC2-617

MCAT Institute
3933 Blue Gum Drive
San Jose, CA 95127

Supersonic Airplane Study and Design

Samson Cheung

Introduction

A supersonic airplane creates shocks which coalesce and form a classical N-wave on the ground, forming a double bang noise termed sonic boom. A recent supersonic commercial transport (the Concorde) has a loud sonic boom (over 100 PLdB) and low aerodynamic performance (cruise lift-drag ratio 7). To enhance the U.S. market share in supersonic transport, an airframer's market risk for a low-boom airplane has to be reduced. Computational fluid dynamics (CFD) is used to design airplanes to meet the dual constraints of low sonic boom and high aerodynamic performance.

During the past year, a research effort was focused on three main topics. The first was to use the existing design tools [1,2], developed in past years, to design one of the low-boom wind-tunnel configurations (Ames Model 3) for testing at Ames Research Center in April 1993. The second was to use a Navier-Stokes code (Overflow) to support the Oblique-All-Wing (OAW) study at Ames. The third was to study an optimization technique applied on a Haack-Adams body to reduce aerodynamic drag.

Ames Model 3

Efforts were made to design a new wing/body/nacelle configuration which had a reduced lower sonic boom relative to the baseline. The baseline configuration, 1080-911 from Boeing Company [3], is a low boom High Speed Civil Transport (HSCT) concept.

The computational code that was used in the design process was a combination of several CFD codes and an optimizer (NPSOL). The computational tools which interconnect in the optimization procedure are listed below:

- UPS3D code: 3-D parabolized Navier-Stokes code [4]
- NPSOL: optimization code
- HYPGEN: hyperbolic grid generator
- LHF: sonic boom extrapolation code based on Whitham's theory
- DB: sonic boom loudness calculation based on Stevens' Mark VII method

This optimization procedure was applied to modify the baseline configuration (1080-911). The result of the optimization was used to build a wind-tunnel model (Ames Model 3). This wind-tunnel model was tested in the Ames 9'x7' wind tunnel in April 1993.

Although the wind-tunnel data of Model 3 has not been released, the CFD calculation shows that the baseline configuration has a loudness level about 100 PLdB; whereas

Model 3 has about 92 PLdB. The results of this research were presented in the Sonic Boom Workshop held at Ames Research Center, May 12-14, 1993 [5]. The presented materials are under ITAR regulation and will be published under restricted distribution. Figure 1 shows the configuration and the flow field of Model 3. The plot at the lower right-hand corner of the figure shows the sonic booms of the baseline and Model 3 respectively.

OAW Study

Oblique flying-wing is an alternative supersonic aircraft concept. Ames, Boeing and Douglas Aircraft Company have joined to form a study group to investigate the feasibility of OAW for commercial use. The study includes aerodynamic performance, stability, structure, landing gear, airplane exits, and airport regulations. The study group has decided to build a wind-tunnel model to test the aerodynamic performance of the airplane.

The CFD portion of this effort was to analyze and design the airfoil shape and deflection of the wing. The flow solver being used was Overflow code, a 3-D Navier-Stokes code using the diagonal with ARC3D algorithm. Figure 2 shows the wings that were analyzed since the beginning of the study in August 1992. Figure 3 shows the optimized results in lift-drag ratio of one of the configurations by optimizing the wing deflection.

Since this study is also under ITAR regulation, the results can only be presented in the weekly group meetings; and no result has been published in any form.

Haack-Adams Body

The purpose of this study was to search for a design method to minimize the drag of a supersonic projectile. The baseline configuration chosen for this study is called Haack-Adams body [6], which is a body of revolution with a pointed nose and a base of finite area. This body has minimum wave drag under slender body theory. Wind-tunnel data are available for CFD validation. The method of optimization makes use of Fourier Sine expansion which has two main advantages over the traditional techniques based on shape functions and control points:

- The volume of the body is fixed without putting external constraints.

  External constraints cost more computational time. For some cases, fixed volume is not feasible.

- Number of design variables is substantially reduced.

  More design variables cost more computational time.

The method of optimization and current results will be published and presented in AIAA 11th Applied Aerodynamics Conference at Monterey, California, August 9-11, 1993. A draft of this paper is attached in the Appendix.

References

1. Cheung, S., Edwards, T., and Lawrence, S.: Application of CFD to Sonic Boom Near and Mid Flow-Field Prediction. J. of Aircraft, Vol. 29, No. 5, 1992.
2. Cheung, S. and Edwards, T.: Supersonic Design Optimization Method for Aerodynamic Performance and Low Sonic Boom. High Speed Research: Sonic Boom, Vol. II, NACA CP-3173, 1992.
3. Haglund, G. and Ogg, S.: Two HSCT Mach 1.7 Low Boom Designs. High Speed Research: Sonic Boom, Vol. II, NACA CP-3173, 1992.
4. Lawrence, S., Chaussee, D., and Tannehill, J.: Application of an Upwind Algorithm to the 3-D Parabolized Navier-Stokes Equations. AIAA paper 87-1112, June 1987.
5. Haack, W.: Projectile Shapes for Smallest Wave Drag. Translation No. A9-T-3, Contract W33-038-ac-15004, ATI No. 27736, Air Material Command, US Air Force, Brown Univ., 1948.

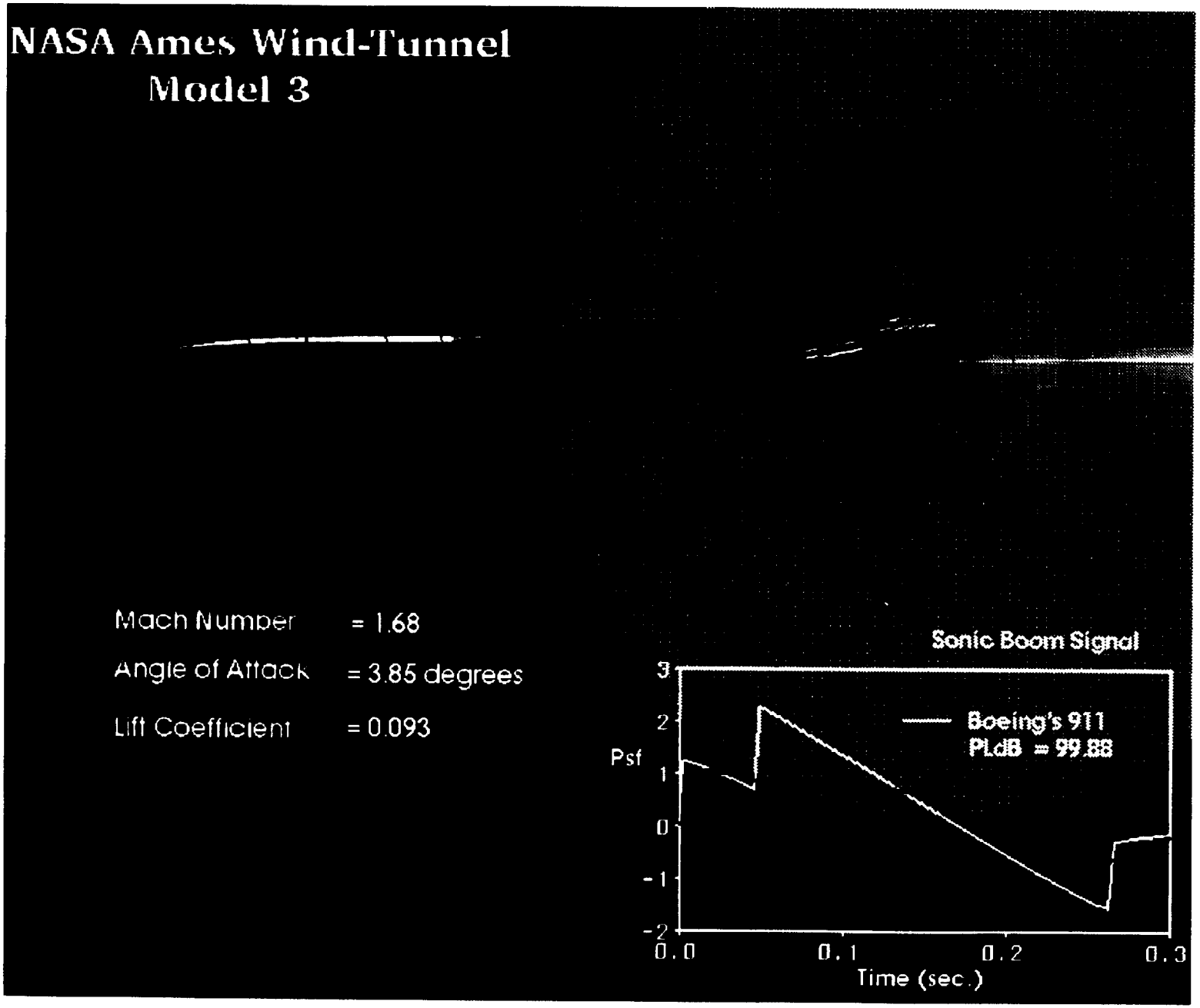
NASA Ames Wind-Tunnel
Model 3
Mach Number = 1.68
Angle of Attack = 3.85 degrees
Lift Coefficient = 0.093
Sonic Boom Signal
Psf
3
2
1
0
-1
-2
0.0
0.1
0.2
0.3
Time (sec.)
Boeing's 911
PLdB = 99.88

Figure 1

OAW Design Evolution, 8/92 - 5/93

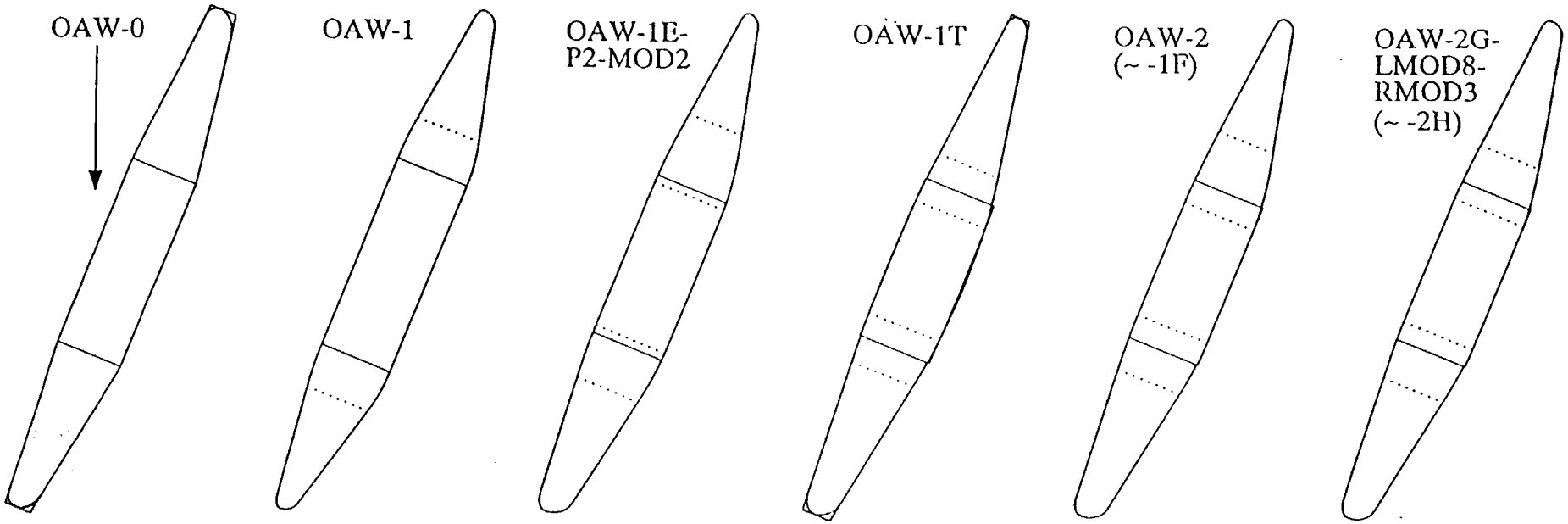

OAW-0	OAW-1	OAW-1E-P2-MOD2	OAW-1T	OAW-2 (~ -1F)	OAW-2G-LMOD8-RMOD3 (~ -2H)
8/92: Baseline study, Waters, et al.	12/92: Larger cabin per initial Boeing req.	2/93: Addresses aft tip separation	3/93: Fully-blended cabin section	3/93: Taper station moved inboard	4/93: 17% cabin per revised Boeing req.
Rectilinear planform with elliptic tips	Parabolically blended planform	Shorter cabin span, asymmetric composite superelliptic/ linear taper; left-tip camber mods.	Superelliptic taper from center with minimum area and volume	Otherwise as for OAW-1E-P2-MOD2; sharp tips fitted via CAD system	Minimum area/ minimum volume composite taper; 12% forward tip with fore/aft droop; revised left tip mods.
T/C 16% everywhere	16% cabin, 8% at tip caps				
Cabin chord 51.4 ft	55.8 ft				
Cabin span 149 ft	152 ft	128.33 ft			
Taper station 74.5 ft	76 ft	58.33 ft	45.83 ft		50 ft
Taper ratios 0.40	0.30	0.45 & 0.25	0.45 & 0.30	0.45 & 0.25	0.45 & 0.30
Aspect ratio 10.0	9.21	9.36	9.58	9.59	9.50

Also:
OAW-2M
has 8/17/8% (stepped cabin)
& OAW-2M has fully blended cabin

DAS/RAK, 5/5/93

(Figure 2)

Optimization of L/D by Bending (OAW-0)

$$(z-z0) = B\%(1/b)(y-y0)^2$$

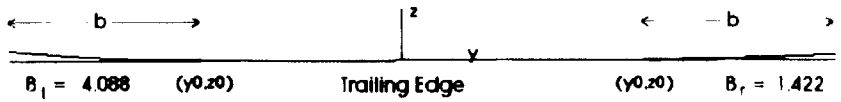

Upper Surface

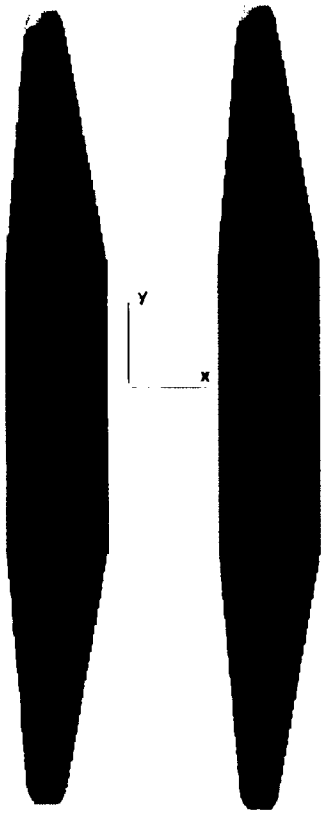

Original Optimized

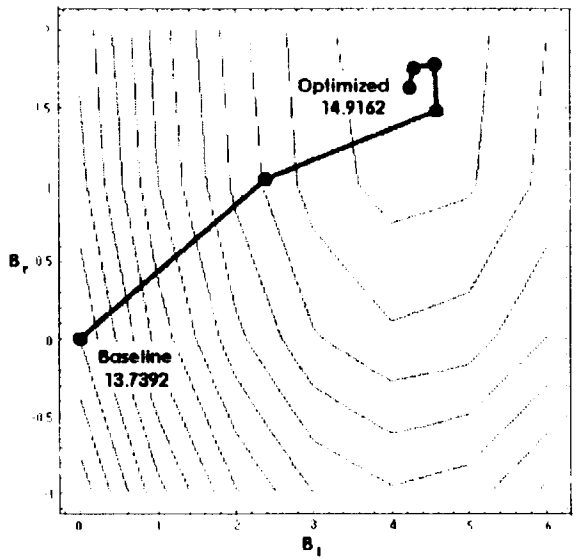

1.E-3	C_L	C_D	C_S	C_{mx}	C_{my}	C_{mz}
Original	113.4	8.2540	14.434	-4.8487	-6.3530	-2.7330
Modified	103.7	6.9533	1.2758	2.2528	-3.9029	-2.4459

Pressure

0.08 0.64 1.21 1.77

Lower Surface

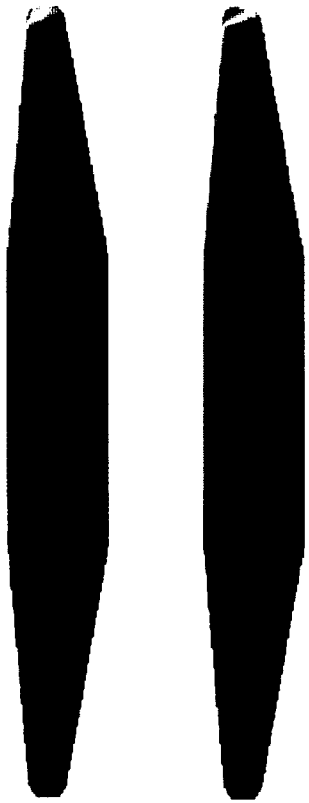

Original Optimized

Figure 3

APPENDIX

CFD OPTIMIZATION OF A THEORETICAL MINIMUM-DRAG BODY

Samson Cheung* and Philip Aaronson**
MCAT Institute
Moffett Field, California

Thomas Edwards†
NASA Ames Research Center
Moffett Field, California

Abstract

The increasing performance and environmental demands required of an aircraft necessitate the need for a set of design tools capable of meeting these challenges. This paper describes the methodology behind coupling a fast, parabolized Navier-Stokes flow solver to a nonlinear constraint optimizer. The design parameters, constraints, grid refinement, behavior of the optimizer, and flow physics related to the CFD calculations are discussed. A theoretical minimum-drag body of revolution is chosen as an initial configuration for the optimization process. For the slender axisymmetric body, a calculation including nonlinear and viscous effects produces a different minimum drag area distribution than linear theory and results in a drag reduction of approximately 4%. This design tool can be used in aerodynamic optimization and sonic boom minimization of supersonic aircraft. The High Speed Civil Transport (HSCT) is a prime example.

Introduction

The need for computational fluid dynamics (CFD) in aerodynamic optimization has been highlighted as the supercomputer plays a significant role in aerodynamic research. One of NASA's research thrusts, the High Speed Research Program (HSRP), defines challenges in sonic boom and aerodynamic optimization. The primary focus is the High Speed Civil Transport (HSCT),[1] which is the next generation supersonic passenger aircraft. In this paper, the techniques and tools of aerodynamic optimization will be described. A theoretical minimum drag body of revolution is chosen as the baseline configuration for the optimization process.

A shape perturbation method is chosen for optimization in the present study. A similar method was used extensively by Haney, Johnson, and Hicks[2] to optimize transonic wings. In their method a potential flow solver was coupled with a feasible direction algorithm. The design variables were the scalar coefficients of a finite set of chosen sine and exponential functions. These functions were then added to the upper surface of the wing, perturbing the wing's shape. Cosentino and Holst[3] coupled the TWING and QNM codes and performed a spline fit across control points located in the upper surface of the wing. In a two-dimensional analysis, Vanderplaats and Hicks[4] coupled a potential code with the constraint optimizer CONMIN. Polynomial coefficients were used as design functions; lift and wave drag were used as test case objective functions. Aero-function shapes were developed through the use of an inverse optimization process by Aidala, Davis, and Mason.[5] These were used with a potential flow code coupled to CONMIN. Each shape was designed to control an aspect of the pressure distribution and then employed as a design variable in the optimization process. The present method takes advantage of a Fourier sine series that defines the original body. The Fourier coefficients make for convenient, physically relevant design variables.

As a test case, the Haack-Adams[6,7,8] (H-A) theoretical minimum drag body of revolution is chosen. The H-A body is selected in this study because it is a classic aerodynamics problem for which validating experimental data[9] are available. Further, because of its simple geometry, running large numbers of permutations is still relatively inexpensive. And since the geometry ends in a finite base, it is particularly well suited for space-marching codes. Also, by including viscous and other nonlinear effects it is hoped that a new optimum may be located.

The H-A body is first derived and then the CFD flow solver is validated on the geometry over a range

* Research Scientist, Member AIAA
** Junior Research Scientist
† Assistant Chief, Computational Aerosciences Branch. Senior Member AIAA

of Mach numbers and grid densities. Then the optimization procedure is described, including optimizer behavior, design variable studies, and the constraints used. Finally, several runs of the optimizer/flow solver are completed on the H-A body and the results are presented.

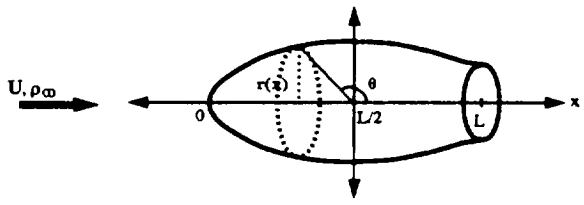

Figure 1. A body of revolution.

Haack-Adams Body

The H-A body is a classic aerodynamic shape derived from supersonic slender body theory. This shape minimizes the wave drag subject to constraints on the volume and base area. The H-A body was chosen as a test case for this approach to optimization. It was chosen for its database of experimental data which can be used as a verification of the CFD code. The simplicity of the geometry makes grid generation relatively easy and robust. The finite base of the H-A body makes for an easier correlation with experimental data, which has an attached sting, and for modeling with space-marching codes.

Slender-body theory, which was used in deriving the H-A body shapes, is a special case of small perturbation potential-flow theory with the additional restriction that the product $r\sqrt{M_\infty - 1}$ is much smaller than x, where r is radius of the body at some streamwise distance x along the axis of the body, and M_∞ is the freestream Mach number. The theory described in this section can be found in most aerodynamic textbooks,[10,11] but is reviewed here for convenience.

Consider supersonic flow of velocity U and density ρ_∞ over a body of revolution of length L as shown in Fig. 1. The velocity potential due to a linear source distribution of strength $Uf(x)$ is

$$\phi(x) = -\frac{1}{2\pi}\int_0^{x-\beta r} \frac{f(\xi)}{(x-\xi)^2 - \beta^2 r^2}\, d\xi$$

where $\beta = \sqrt{M_\infty - 1}$ and $x = L(1+\cos\theta)/2$. Expressing f as a Fourier sine series,

$$f(\theta) = L\sum_{n=1}^{\infty} \alpha_n \sin(n\theta)$$

The derivative of the cross-sectional area, (A') can be approximated by f. Integrating f produces,

$$A(\theta) = \int_\pi^\theta f(\theta)d\theta$$

$$= -\frac{L^2}{2}\int_\pi^\theta \sum_{n=1}^{\infty} [\alpha_n \sin(n\theta)][\sin\theta]d\theta$$

$$A(\theta) = \frac{L^2}{4}\left\{\alpha_1(\pi - \theta + \frac{1}{2}\sin 2\theta) + \alpha_2\frac{4}{3}\sin^3\theta + \sum_{n=3}^{\infty}\alpha_n\left(\frac{\sin(n-1)\theta}{n-1} - \frac{\sin(n+1)\theta}{n+1}\right)\right\} \quad (1)$$

Slender-body theory gives the formula of wave drag,

$$D_w = \frac{\pi\rho_\infty U^2 L^2}{8}\sum_{n=1}^{\infty} n\alpha_n^2 \quad (2)$$

Equations (1) and (2) show that the cross-sectional area and the wave drag are only dependent on the Fourier coefficients α_n, not the Mach number. The H-A body is defined by the body shape that minimizes D_w subject to the following conditions:

- C1 ≡ the area at the base $A(L) = A_{base}$ is fixed and non-zero
- C2 ≡ zero slope at the end, $\left(\frac{dA}{dx}\right)\Big|_{x=L} = 0$
- C3 ≡ the location of maximum thickness, x_{max}, is fixed

It is easy to check that Eq. (1) satisfies C2. The remaining two conditions C1 and C3 determine the values of α_1 and α_2. In order for a body to produce minimum drag, Eq. (2) suggests that $\alpha_n = 0$ for $n \geq 3$. Condition C1 gives

$$\alpha_1 = \frac{4A_{base}}{L^2\pi} \quad (3)$$

and C2 gives

$$\alpha_2 = \frac{\alpha_1}{2\cos\theta_{max}} \quad (4)$$

Optimization Procedure

The optimizer first generates a baseline objective function from the initial values of the design variables supplied as input. The optimizer then perturbs each of the design variables in order to locate a search direction. During each perturbation, a surface grid and volume grid are generated. The flow is then solved on the volume grid and from this, the objective function is produced. The optimizer continues to perturb and search until a set of design variables, and thus a new body shape, is obtained with a local minimum objective function (see Fig. 2). With NPSOL, both linear and nonlinear constraints can be added to the design variables.

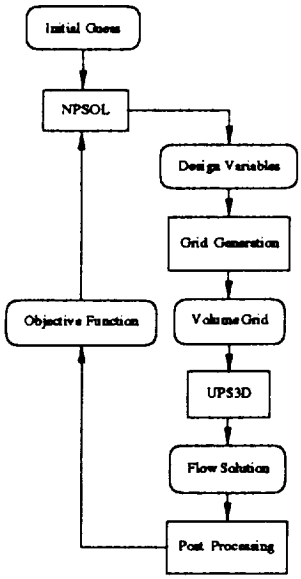

Figure 2. Diagram of optimization procedure.

Design Variables

Perturbations are performed through the use of design variables that have a direct influence on the objective function. The design variables used here were inspired by the original Fourier sine series used in the derivation of the H-A body. Equation (1) can be rewritten using Eqs. (3) and (4) as

$$\frac{r^2}{r_{max}^2} = \frac{A_{base}}{\pi A_{max}}\left\{(\pi - \theta + \frac{1}{2}\sin 2\theta) + \gamma_1 \frac{4}{3}\sin^3\theta + \sum_{m=2}^{\infty}\gamma_m\left(\frac{\sin(m)\theta}{m} - \frac{\sin(m+2)\theta}{m+2}\right)\right\} \quad (5)$$

where $\gamma_m = \alpha_m/\alpha_1$ for $m = 2, 3, \ldots$ Where r_{max} and A_{base}/A_{max} are known. According to linear theory γ_m $m = 2, \ldots, N$ are set to zero. However, since nonlinear effects are included in the CFD analysis, these coefficients were chosen as the design variables. Therefore, the optimized configuration will also be defined by Eq. (5).

Constraints

It is important to check that this optimal configuration satisfies the three conditions (C1, C2, and C3) of the H-A body. Equation (5) satisfies C1 when evaluated at $\theta = 0$ and $(dA/dx = \pi d(r^2)/dx)$.

$$\frac{dA}{d\theta}\frac{d\theta}{dx} = -\pi\frac{2A_{base}}{L\pi A_{max}}\left\{-\frac{2\sin^2\theta}{\sin\theta} + \gamma_1\frac{4\sin^2\theta\cos\theta}{\sin\theta} + \sum_{m=2}^{\infty}\gamma_m\left(\frac{\cos(m)\theta - \cos(m+2)\theta}{\sin\theta}\right)\right\} \quad (6)$$

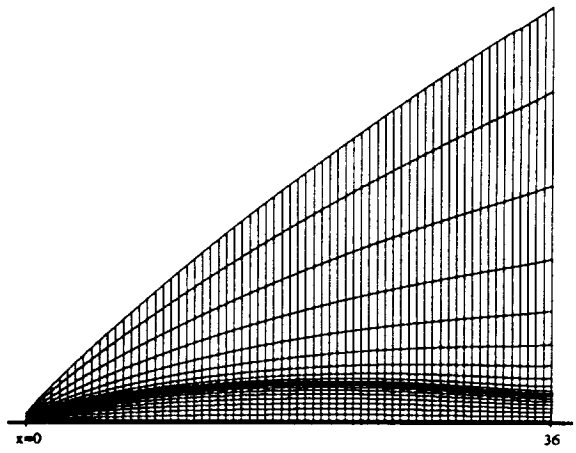

Figure 3. Haack-Adams, UPS marching grid with a number of the planes omitted for simplicity.

Equation (6) is zero when evaluated at $\theta = 0$. Note that the terms inside the summation sign are zero by L'Hôpital's Rule, thus, C2 is satisfied. Condition C3 requires the H-A body to satisfy $(dA/dx)|_{x=x_{max}} = 0$. In the optimization process, the location of the maximum was allowed to change in such a way that $-1 \leq (dA/dx)|_{x=x_{max}} \leq 1$, that is

$$\left|-2\sin^2\theta_{max} + 4\gamma_1\sin^2\theta_{max}\cos\theta_{max} + \sum_{m=2}^{\infty}\gamma_m\left(\cos(m)\theta_{max} - \cos(m+2)\theta_{max}\right)\right| \leq 1 \quad (7)$$

where $\theta_{max} = \cos^{-1}(2x_{max}/L - 1)$. This constraint effectively allows x_{max} (or θ_{max}) to shift by a small amount, whereas on the original H-A body x_{max} is fixed. An additional requirement is needed to ensure that the radius of the optimal body (Eq. (5)) is always greater than or equal to zero; that is,

$$(\pi - \theta + \frac{1}{2}\sin 2\theta) + \gamma_1\frac{4}{3}\sin^3\theta + \sum_{m=2}^{\infty}\gamma_m\left(\frac{\sin(m)\theta}{m} - \frac{\sin(m+2)\theta}{m+2}\right) \geq 0 \quad (8)$$

for all $0 \geq \theta \geq \pi$. Equations (7) and (8) set the relationships among the γ's and are treated as constraints for the optimization problem.

Flow Solver

The implemented CFD flow solver is the 3-D parabolized Navier-Stokes code, UPS3D.[12] This is a space-marching code that calculates steady-state viscous or inviscid solutions to supersonic flows. A conic approximation is made for the initial marching plane. This code is further supported by a hyperbolic grid

generation scheme[13] that is sufficiently fast and robust to operate within an automated optimization environment. In this study, both viscous and inviscid supersonic calculations are employed. From these solutions, the drag coefficient C_D is calculated by integrating pressure and skin friction (if applicable) over the surface of the body.

The UPS3D code uses a step size of 0.1% of the body length (L) on a grid of 21 points in the circumferential direction and 50 points in the body-normal direction. The grid points are clustered near the body surface (see Fig. 3).

Objective Function

Five design variables, namely, $\gamma_2, \gamma_3, ..., \gamma_6$ of Eq. (5) are used in the majority of the remainder of this study. At each step, the optimizer alters the values of the γ's and a new shape is defined. A new computational grid is then created and UPS3D calculates the flow over this new geometry. The wave drag coefficient (C_{D_w}) is determined by numerical integration of the pressure coefficient (C_p) over the body

$$C_{D_w}(x) = \iint \frac{C_p}{A_{max}} dS(x) = \int_0^x \frac{2\pi r C_p}{A_{max}} \left(\frac{dr}{dx}\right) dx$$

If skin friction as well as pressure is included in the integration then total drag is calculated.

Optimizer

The optimizer, NPSOL,[14] is a collection of Fortran subroutines designed to solve the nonlinear programming problem:

$$\text{minimize } F(x)$$

$$\text{subject to : } l \leq \begin{bmatrix} x \\ Ax \\ c(x) \end{bmatrix} \leq u$$

where $F(x)$ is the objective function, x is a vector of length n that contains the design variables, $c(x)$ contains the nonlinear constraint functions, and A is the linear constraint matrix. Note that u and l, the upper and lower bounds, are vectors and thus are specified for each variable and constraint.

NPSOL uses a sequential quadratic programming algorithm to look for the minimum of $F(x)$. Within each iteration, the search direction is the solution of a quadratic programming (QP) algorithm. Each QP subproblem is solved by a quasi-Newton approximation. The optimizer stops when it finds a local minimum of $F(x)$.

The user needs to define $F(x)$, A, $c(x)$ and the bounds for each, as well as an initial estimate of the solution. An important consideration is the difference interval used in the finite difference approximation of the gradient. NPSOL has an option to calculate the difference interval; however, this involves a large number of calls to the flow solver, which is impractical. The difference interval is specified as an input throughout this study.

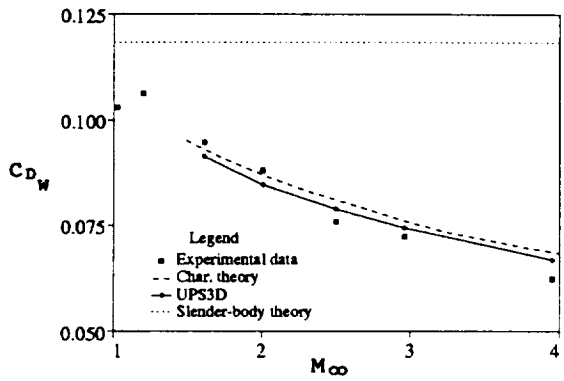

Figure 4. Wave drag comparison over a range of Mach numbers. $\frac{L}{2R_{max}} = 7$

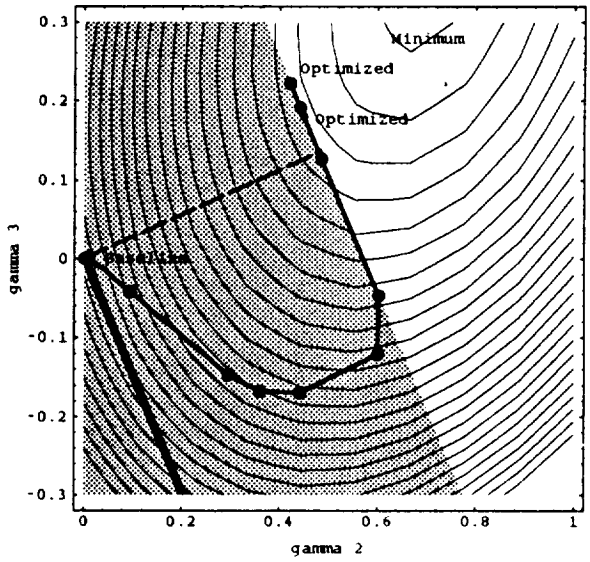

Figure 5. Constrained optimization paths for a difference interval of $\Delta\gamma = 0.01$ (solid line) and $\Delta\gamma = 0.005$ (dashed line).

Results and Discussion

Test Case

As a validation test case, the UPS3D code run in inviscid mode is compared against the experimental data. A review of Fig. 3 illustrates a typical grid used by UPS3D, which shows the surface as well as a plane normal to the body. In the experimental study,[9] the H-A body had a length L of 36" with a fineness ratio $L/2r_{max}$ of 7. The location of maximum thickness was $x_{max} = 21"$ ($\theta_{max} = \cos^{-1}(\frac{1}{6})$), and $A_{base}/A_{max} = 0.532$.

The UPS3D code was tested over a range of supersonic Mach numbers and compares well with characteristic theory and experimental data (see Fig. 4). Note the variation of wave drag with Mach number predicted by both the characteristic theory and inviscid CFD solutions. Slender body theory predicts no variation of drag with Mach number (see Eq. 2).

In order to first visualize the process of optimization, a two-design-variable (γ_2 and γ_3) case is considered. Figure 5 is a contour plot of the wave drag coefficient with respect to γ_2 and γ_3. The dots in the figure are iterative points in the optimization. Linked together, they form a search path. The thickest solid line satisfies the equation $(dA/dx)|_{x=x_{max}} = 0$, and the shaded area satisfies the inequality $-1 \leq (dA/dx)|_{x=x_{max}} \leq 1$, (Eq. (7)), which is the constraint used. Both the thinner solid line and the dashed line are search paths used by NPSOL with difference intervals of $\Delta\gamma = 0.01$ and $\Delta\gamma = 0.005$, respectively. The larger difference interval calculates a less accurate gradient and thus locates a minimum more slowly than the smaller difference interval. However, there are two local minima in this design space along the constraint boundary. The larger difference interval found the better of the two minima. The smaller difference interval stopped before it found that minimum. This is not always the case as a larger difference interval could miss a local minimum by "stepping" over it entirely.

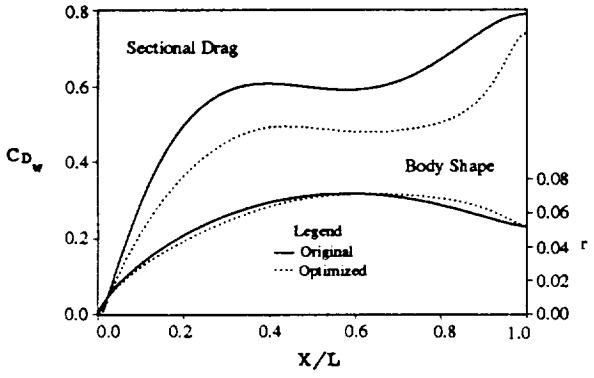

Figure 6. Inviscid optimization with five design variables. $M_\infty = 2.5$ $\frac{L}{2R_{max}} = 7$

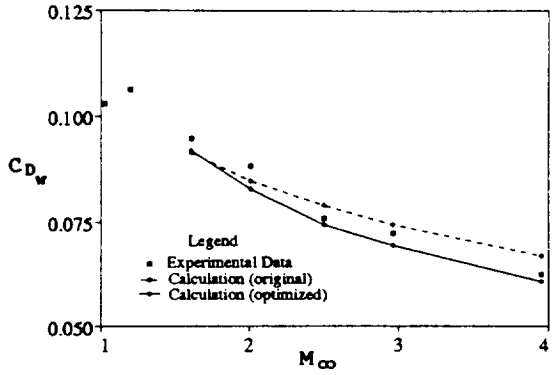

Figure 7. Wave drag comparison between the original H-A body and the H-A body optimized at $M_\infty = 2.5$, over a range of Mach numbers. $\frac{L}{2R_{max}} = 7$

Inviscid Optimization

The inviscid optimization process gave the result shown in Fig. 6 for a freestream Mach number of 2.5 and an angle of attack of zero deg. The sectional wave drag coefficient is plotted along with the radius of the original and optimized shapes. The volume of the forebody is reduced by NPSOL in order to improve the sectional wave drag in this region. The improvement over the original H-A body is reduced aft of the maximum cross-sectional area because of an increase in volume that occurred satisfying the constraints (C1 and C2). Overall, the wave drag of the Haack-Adams body was reduced by 5%. Although the optimized body was designed at Mach 2.5, Fig. 7 shows that the same optimized body gives lower drag than the H-A body at other Mach numbers. Using $\Delta\gamma = 0.01$, 48 new body shapes were generated and analyzed to reach this result. The whole process took approximately 2.5 CPU hours on the Cray-YMP. Each flow solution calculated by UPS3D uses 160 sec, with an additional 1.3 sec in grid generation.

Viscous Optimization

The same design procedure was also performed with viscosity taken into account. The result is shown in Fig. 8. The optimizer took much the same strategy as the inviscid case in that the nose of the body was reduced, while a penalty was paid at the rear of the body. The viscous drag results include both wave and skin friction drag, so while the actual drag reduction is comparable to the inviscid optimization, the improvement in this case is 4%. Figure 9 shows that the same body gives lower drag than the original at other Mach numbers. This optimization process with $\Delta\gamma = 0.01$ took about 3.5 CPU hours total on the

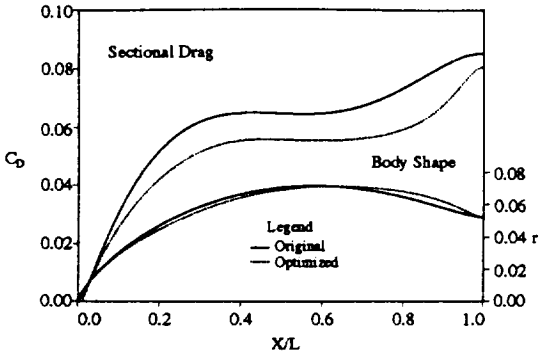

Figure 8. Navier-Stokes optimization with five design variables. $M_\infty = 2.5$, $\frac{L}{2R_{max}} = 7$, $Re = 9 \times 10^6$

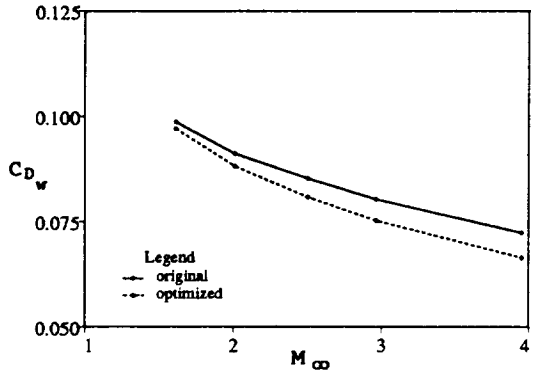

Figure 9. Total drag comparison between the original H-A body and the H-A body optimized with 5 design variables at $M_\infty = 2.5$, over a range of Mach numbers. $\frac{L}{2R_{max}} = 7, Re = 9 \times 10^6$

Cray-YMP and employed 40 flow solutions. Each solution took UPS3D 320 sec with an additional 1.3 sec utilized in grid generation. The following table gives the values of the design variables for the inviscid and viscous optimization processes:

Haack-Adams Body $M\infty = 2.5$					
	γ_2	γ_3	γ_4	γ_5	γ_6
Inviscid	0.853	0.673	0.495	0.420	0.0846
Viscous	0.679	0.598	0.353	0.264	0.01875

Off-Design Performance

The effects of off-design angle of attack and Reynolds number on the performance of the new, optimized shape were also investigated. For the body that was optimized at zero angle of attack, the effects of nonzero angles of attack are shown in Fig. 10. As α increases, the reduction of drag versus the original decreases slightly.

The lower half of Fig. 11 indicates the radial distribution results of three optimization processes at differing Reynolds numbers. The solid line is the original H-A body, the dashed line is the body optimized at a Reynolds number of 10^6, and the dotted line is the body optimized at a Reynolds number of 10^5. The sectional total drag coefficient of these three configurations calculated at a Reynolds number of 10^6 is shown in the upper half of the figure. The lower Reynolds number case, which features thicker boundary layers, and hence greater flow displacement, shows the largest perturbation in geometry from the H-A body.

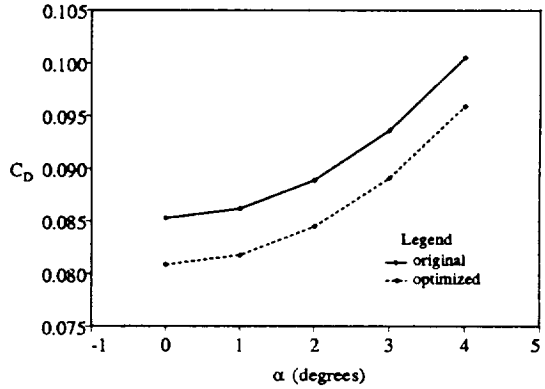

Figure 10. Total drag comparison between the original H-A body and the H-A body optimized with 5 design variables at $M_\infty = 2.5$ and $\alpha = 0$, over a range of α. $\frac{L}{2R_{max}} = 7$, $Re = 9 \times 10^6$

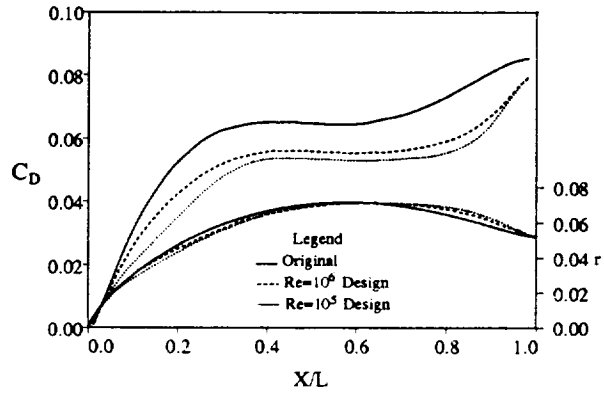

Figure 11. Total drag comparison between the original H-A body and H-A bodies optimized with 5 design variables at $M_\infty = 2.5$ and $\alpha = 0$, over a range of Re numbers. $\frac{L}{2R_{max}} = 7$

Grid Refinement

A calculation performed on a coarse grid will, in general, contain a larger numerical error than one performed on a fine grid. However, the coarser grid will, in most cases, run significantly faster. It is desirable to reduce the computer time by using the coarsest grid possible that will still yield a physically accurate result. The key to running an optimizer/flow solver efficiently is to choose a sufficiently coarse grid that the cumulative CPU time does not become excessive, yet a fine enough grid to locate a physically valid optimum.

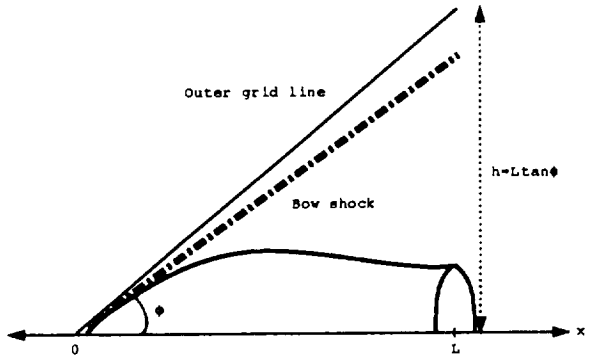

Figure 12. Relationship between the size of the computational grid and the bow shock.

In this grid-refinement study, an optimization problem at Mach 2.5 and zero-degree angle of attack was considered. The computational grid had 21 points in the circumferential direction and the step size of the UPS3D code was taken to be 0.1% of the body length. The grid resolution in the circumferential direction and the step size were fine enough to be kept fixed; only the number of grid points (P) in the normal direction was altered. The distance between the first grid point (in the normal direction) and the surface grid is less than or equal to $s = 0.5(h/P)$, where h, given by $L\ \tan(\phi)$, is the vertical distance from the end of the body to the outer grid (see Fig. 12). Due to grid effects, the calculated bow shock position of the H-A body differed with grid density until the grid was dense enough to resolve the physical shock location. For each computational grid, the angle ϕ was chosen so that the bow shock was as close as possible to the outer boundary. The table below gives the values of ϕ and s with different computational grids.

Grid Points (P)	ϕ (degree)	Spacing (s/L)
10	50	0.060
20	42	0.025
30	38	0.013
40	36	0.009
50	32	0.006
60	31	0.005
70	30	0.004
95	30	0.003

The behavior of the flow solution and optimization results on the various grids are analyzed to characterize the errors arising from grid density. For clarification, the following definitions are introduced:

$D(P) \equiv C_D$ calculated on a P-point H-A grid.

$D(\infty) \equiv C_D$ calculated on an asymptotic H-A grid (approximated by 95 points).

$D^m(P) \equiv C_D$ calculated on a P-point grid whose surface shape is obtained in an optimization process on an m-point grid.

$\Delta D^m(\infty) \equiv |D^m(\infty) - D(\infty)|$ the drag reduction of new design which was obtained by the optimization process on an m-point grid.

$\Delta D^\infty(\infty) \equiv |D^\infty(\infty) - D(\infty)|$ the actual drag reduction of the new design.

The errors due to grid density in the CFD computations of the H-A body and the optimized design are given by $|D(P) - D(\infty)|$ and $|D^P(P) - D^P(\infty)|$, respectively. Both curves are plotted in Fig. 13 and show a roughly exponential decay in error due to grid density. Fig. 14 reveals the grid effect in the optimization process and the CFD calculations. The dashed curve is the error due to grid density in the optimization process, given by $|\Delta D^n(\infty) - \Delta D^\infty(\infty)|$. The solid curve is the error due to grid density in optimization and the CFD calculation, given by $|\Delta D^n(n) - \Delta D^\infty(\infty)|$. This figure indicates that the optimization process does not require an overly fine grid in order to locate a physical optimum.

The grid used in the optimization process still has to be fine enough to capture the flow properties and relevant physics in order to obtain a grid independent optimum. For example, if the grid with $P = 30$ is used, the computed bow-shock is too far

away from the exact location, and thus the optimized result has an understandably large error. If the grid with $P = 50$ is used, the flow physics is much more realistically approximated, and the optimized result has a much smaller error (compare the error at $L = 50$ in Fig. 14).

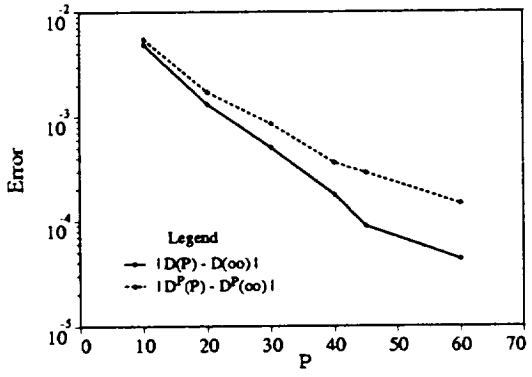

Figure 13. Comparison of the error due to grid density (normal direction) of the original body vs. the modified body. The modified body has been optimized at each of the normal point grids.

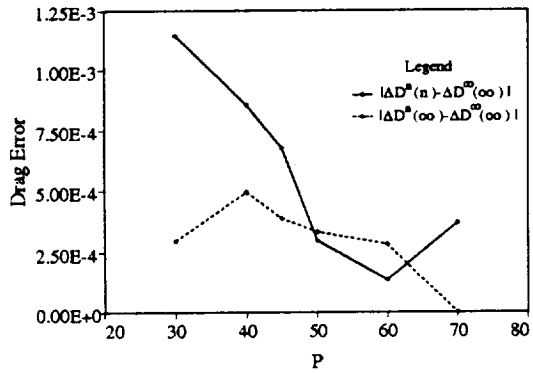

Figure 14. The effects of the number of grid points in the normal direction on the optimization process

Design Variables

As the number of design variables increases, so do the degrees of freedom of the optimization process. Often the larger the number of design variables in the optimization process, the larger the reduction in drag. Figure 14displays the optimized C_{Dw}, from inviscid flow solutions with $M_\infty = 2.5$ under different numbers of design variables. Each square in the figure represents the drag coefficient obtained from the optimization process with an initial guess of $\gamma_i = 0$, $i = 1...n$. Thus as a baseline, the original H-A body is employed. Each diamond represents an initial guess of $\gamma_i = 0.1$, $i = 1...n$. For the case with three and six design variables, the optimized C_{Dw} does not quite follow the expected reduction in C_{Dw}. This is due to a local minimum around the baseline H-A body for those sets of design variables. MORE*

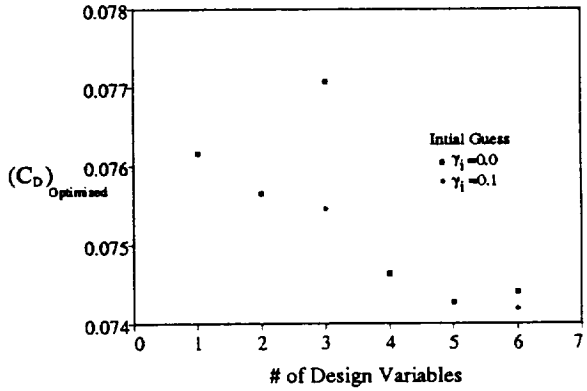

Figure 15. The effects of number of design variables and their initial values on the optimized wave drag. $M_\infty = 2.5$, $\frac{L}{2R_{max}} = 7$

Conclusion

Because of its generality, CFD offers the aircraft designer the opportunity to address many design issues simultaneously. An added advantage is that the geometry definition and performance data are common to any analysis or optimization problem. The theory and implementation of these techniques have been used to optimize both sonic boom and aerodynamic efficiency for a recently developed HSCT type configuration. This paper has demonstrated how the same computational tools can be used to minimize drag coefficient of the Haack-Adam body. The wave drag is reduced by 5%, and the total drag coefficient is reduced by 4%.

The grid refinement study indicates that one does not have to use an overly fine grid in the optimizer/flow solver operation in order to obtain an accurate optimal body shape. However, the grid has to be fine enough to reasonably capture the relevant physics.

References

1. First Annual High-Speed Research Workshop, NASA CP-10087, Part 1, Williamsburg, Virgina, May 14-16, 1991.
2. Haney, H. P., Johnson, R. R., and Hick, R. M., "ComputationalOptimization and Wind Tunnel Test of Transonic Wing Designs", AIAA paper 79-0080, Jan., 1979.

3. Cosentino, G. B. and Holst, T. L., "Numerical Optimization Design of Advanced Transonic Wing Configurations", NASA TM 85950, May 1984.

4. Vanderplaats, G. N., and Hicks, R. M., "Numerical Airfoil Optimization Using a Reduced Number of Design Coordinates", NASA TM X-73,151, July 1976.

5. Aidala, P. V., Davis, W. H. Jr., and Mason, W. H., "Smart Optimization", AIAA paper 83-1863, July 1983.

6. Adams, A. C., "Determination of Shapes of Boattail Bodies of Revolution for Minimum Wave Drag", NACA TN-2550, 1951.

7. Haack, W., "Projectile Shapes for Smallest Wave Drag", Translation No. A9-T-3, Contract W33-038-ac-15004 (16351), ATI No. 27736, Air Force Materiel Command, U.S. Air Force, Brown Univ., 1948.

8. Sears, W. R., "On Projectiles with Minimum Wave Drag", Quart. Appl. Math., vol. IV, no. 4, Jan., 1974, pp. 361-366.

9. Harris, R. and Landrum, E., "Drag Characteristic of a Series of Low-Drag Bodies of Revolution at Mach Numbers from 0.6 to 4.0", NASA TN D-3163, Dec., 1965.

10. Ashley, H. and Landahl, M., *Aerodynamics of Wings and Bodies*, Addision-Wesley, 1965.

11. Sears, W., *General Theory of High Speed Aerodynamics - Part C: Small Perturbation Theory*, High Speed Aerodynamics and Jet Propulsion, Vol. VI, Prinston University Press, 1954.

12. Lawrence, S., Chaussee, D., and Tannehill, J., "Application of an Upwind Algorithm to the 3-D Parabolized Navier-Stokes Equations", AIAA paper, 87-1112, June 1987.

13. Chan, W. and Steger, J., "A Generalized Scheme for Three-Dimensional Hyperbolic Grid Generation", AIAA paper, 91-1588, June, 1991.

14. Gill, P., Murray, W., Saunders, M., and Wright, M., "User's Guide for NPSOL: A Fortran Package for Nonlinear Programming", Tech. Report SOL 86-2, Dept. of Operations Research, Stanford University, 1986.